BOUNDARY CONDITION IDENTIFICATION FOR OETHOTROPIC HEAT CONDUCTION PROBLEMS BASED ON HYBRID TREFFTZ FINITE ELEMENT METHOD WITHOUT ITERATION

Wenkai QIU, Haolong CHEN, and Huanlin ZHOU*

School of Civil Engineering, Hefei University of Technology, Hefei 230009, P. R. China

* Corresponding author; E-mail: zhouhl@hfut.edu.cn

It is essential to accurately identify the boundary condition of pipeline's inner wall in engineering analysis and calculation. An efficient non-iterative algorithm based on the hybrid Trefftz finite element method (HT-FEM) is presented to determine the boundary condition of the inner wall for orthotropic media heat conduction problems. The temperature of measurement points is obtained by solving the forward heat conduction problems using the HT-FEM to simulate the experimentally measured data. The evaluated temperature at these points can be formulated as a function of the temperature of the inner boundary nodes, whose boundary conditions remain to be determined. The objective function is established to quantify the deviation between the measured and evaluated temperature at measurement points by utilizing the least-squares approach. The unknown inner boundary conditions are determined by minimizing objective function. Four numerical examples are provided to analyze the inversion results for different types of pipes. The effects of various factors, encompassing the number and location of measurement point, measurement errors, and mixed boundary conditions on inversion results are discussed. The findings demonstrate that the proposed algorithm exhibits high computational efficiency and accuracy in identifying boundary conditions.

Key words*: non-iterative algorithm, hybrid Trefftz finite element method, boundary condition identification, orthotropic heat conduction problems*

1. Introduction

The inverse heat conduction problems (IHCP) are a critically important category in engineering applications, where it evaluates cause features from the observed outcomes. Usually, this problem can be solved through analytical [1] and numerical methods. However, owing to the inherent limitations of analytical solutions, numerical methods have gained broader applicability. The typical numerical methods include finite element method (FEM) [2, 3], finite difference method (FDM) [4], meshless method [5] and boundary element method (BEM) [6, 7]. Furthermore, depending on the research objectives, IHCPs can be classified

into multiple categories, encompassing inverse physical parameter problems [8-10], inverse heat source problems [11], geometric shape reconstruction [12, 13], and boundary condition identification [14, 15]. The application of numerical methods for boundary condition identification offers a viable alternative to experimental measurements, significantly reducing measurement costs in engineering applications. Consequently, the development of an efficient numerical algorithm for identifying boundary conditions holds not only theoretical research significance, but also provides convenience in solving engineering problems.

The HT-FEM has proven to be both successful and widely applicable in addressing direct engineering problems [16-19], emerging as an efficient numerical tool. In contrast to the traditional FEM, the HT-FEM employs a dual interpolation strategy, encompassing the internal temperature fields within element domains and frame fields defined along element boundaries. This greatly improves computational accuracy. Furthermore, the proposed method shows satisfactory mesh distortion immunity [17]. However, to the authors' knowledge, there have been limited applications of this method in inverse problems, and research on its utilization in identifying boundary conditions has yet to be reported. Therefore, exploring the application of HT-FEM for identifying boundary condition of pipeline's inner wall represents a highly meaningful endeavor.

Generally, the majority of inversion algorithms utilized for addressing inverse problems, encompassing regularization techniques, gradient-based algorithms, intelligent search algorithms, and neural network algorithms, necessitate an iterative procedure. Karnal and Batul [20] used conjugate gradient method (CGM) with an adjoint problem-based function estimation iterative technique to determine the heat flux and internal wall temperature at the throat section of the nozzle. Frackowiak *et al*. [21] utilized CGM and Tikhonov regularization to estimate the thermal boundary condition for 2D IHCP. Sun and He [22] estimated the boundary temperature and heat flux of 3D heat conduction model using fundamental solution meshless method and regularization method. Tourn *et al*. [23] adopted the total variation regularization strategy to estimate surface heat flux for 1D linear IHCP. Chen *et al*. [24] identified time-varying boundary conditions for 2D transient heat conduction problem using improved cuckoo search algorithm and the dual reciprocity BEM. Wang *et al*. [25] determined temperature-dependent thermal conductivity of charring ablator using genetic algorithm and cubic spline interpolation. Udayraj *et al*. [26] identified the unknown boundary heat fluxes by employing three metaheuristic algorithms. Sun *et al*. [27] used an improved krill swarm algorithm to determine temperature-dependent material thermal properties. Yang *et al*. [28] developed a modified CGM to estimate the thermophysical parameters of the transient heat conduction problem, which is crucial for the analysis of composite material in aerospace engineering. Ghadimi *et al*. [29] used artificial neural networks (ANN) and sequence function to evaluate the absorbed heat flux of locomotive brake discs. Gu *et al*. [30] identified transient surface heat flux during pool boiling processes by employing generative adversarial networks.

Although iterative algorithms often exhibit high calculation accuracy, they are plagued by computational inefficiency. This is primarily because of the inherent complexity of the iterative process itself and the iterative errors that arise during calculation. Nevertheless, non-iterative algorithms provide a compelling alternative. They are more competitive,

primarily owing to their superior computational efficiency and, in certain aspects, enhanced accuracy. Su and Chen [31] used virtual domains and rearranged the partial differential equation matrix forms via FDM to determine the boundary geometry of a two-walls furnace. Su *et al*. [32] adopted a non-iterative approach, based on grey prediction model, to determine the geometric shape of the inner surface of furnace wall. Yu *et al*. [33] developed a non-iterative scheme based on BEM to estimate unknown boundary conditions of the furnace inner wall. Qiu *et al*. [34] introduced the concept of virtual domain and developed a non-iteration method based on HT-FEM to determine unknown inner boundary geometry shape. Inspired by prior research, the present work is the first to employ a non-iterative algorithm, grounded in the HT-FEM, for identifying thermal boundary conditions in orthotropic heat conduction problems. The temperatures at inner boundary nodes are determined by reorganizing the stiffness matrix.

The structure of the remaining sections of this paper is outlined as follows. In **Section 2**, the basic formula derivation, the direct and inverse problems are discussed. In **Section 3**, Several numerical examples are adopted to verify the feasibility of the present method. Finally, the conclusion of this paper is provided in **Section 4**.

2. The basic formulas and models

2.1. Problem description

The non-iterative inversion algorithm proposed in this paper is developed based on the formulation of the corresponding direct problem. The analysis is conducted on a 2D pipeline section model, where the material is assumed to exhibit orthotropic properties, as depicted in **Figure 1**. The material property and geometry configuration of the entire model are known. The outer boundary condition $\overline{T}_o$ is prescribed as known, while the inner boundary condition $\overline{T}_i$ remains unknown and serves as the key quantity to be identified in this research.

The governing equation for orthotropic heat conduction problems can be written as

$$k_{11}\frac{\partial^2 T}{\partial x_1^2}+k_{22}\frac{\partial^2 T}{\partial x_2^2}=0 \quad \text{in} \quad \Omega \tag{1}$$

where k_{11} and k_{22} denote the thermal conductivity, and T is the temperature. Ω indicates the solution domain enclosed by boundary $\Gamma=\Gamma_o\cup\Gamma_i$. The Dirichlet and Neuman boundary conditions are given by

$$T=\overline{T}_o \quad \text{on} \quad \Gamma_o \tag{2}$$

$$T=\overline{T}_i \quad \text{on} \quad \Gamma_i \tag{3}$$

$$q=\overline{q} \quad \text{on} \quad \Gamma_i \tag{4}$$

where $\overline{T}_o$ represents the temperature imposed to the boundary Γ_o, $\overline{T}_i$ is the unknown temperature at the boundary Γ_i, and $\overline{q}$ is the unknown heat flux on the boundary Γ_i.

2.2. Direct Problems

The HT-FEM is adopted to solve the direct problem, thereby facilitating the acquisition of measured temperature at measurement points. As illustrated in **Figure 2**, compared to

conventional FEM, this method adopts a dual interpolation approach. Specifically, it interpolates both the temperature fields in inner element domains and frame fields defined along element boundaries.

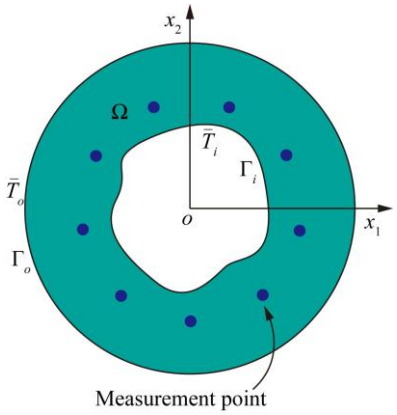

Figure 1. Pipeline section model

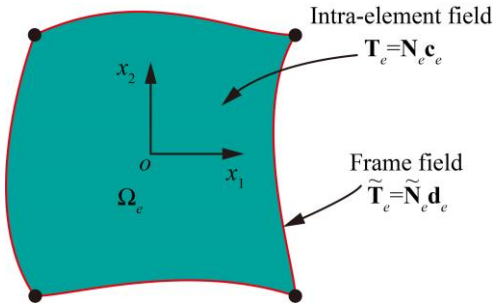

Figure 2. HT-FEM element model

The internal element temperature filed of the HT-FEM can be given by

$$T_e(\mathbf{x})=\sum_{j=1}^{n}N_{ej}c_{ej}=\mathbf{N}_e(\mathbf{x})\mathbf{c}_e \tag{5}$$

where N_{ej} represents the complete solution system for orthotropic heat transfer, c_{ej} is the coefficient to be determined, and n is the number of terms of the truncated complete solution system.

The frame temperature field is written as

$$\tilde{T}_e(\mathbf{x})=\tilde{\mathbf{N}}_e(\mathbf{x})\mathbf{d}_e(\mathbf{x}) \tag{6}$$

where $\tilde{\mathbf{N}}_e$ represents shape function vector of linear interpolation, $\mathbf{d}_e$ denotes degree-of-freedom vector of the element node.

Then, the modified variational functional [16-19] is constructed to link the two temperature fields and can be given by

$$\Pi_m=\sum_e\Pi_{me} \tag{7}$$

where

$$\Pi_{me}=\frac{1}{2}\int_{\Omega_e}k_{ii}T_{e,i}T_{e,i}\mathrm{d}\Omega-\int_{\Gamma_{eT}}q_e\bar{T}_e\mathrm{d}\Gamma+\int_{\Gamma_{eq}}(\bar{q}_e-q_e)\tilde{T}_e\mathrm{d}\Gamma-\int_{\Gamma_{eI}}q_e\tilde{T}_e\mathrm{d}\Gamma \tag{8}$$

where $T_{e,i}$ is partial derivative of temperature in the coordinate direction, $\bar{T}_e$ and $\bar{q}_e$ represent known temperature and heat flux, $\tilde{T}_e$ denotes frame temperature. After introducing the Gaussian divergence theorem, it can be further deduced that

$$\Pi_{me}=\frac{1}{2}\mathbf{c}_e^{\mathrm{T}}\mathbf{H}_e\mathbf{c}_e+\mathbf{d}_e^{\mathrm{T}}\mathbf{P}_e-\mathbf{c}_e^{\mathrm{T}}\mathbf{G}_e\mathbf{d}_e \tag{9}$$

in which

$$\mathbf{H}_e=\int_{\Gamma_e}\mathbf{Q}_e^{\mathrm{T}}\mathbf{N}_e\,\mathrm{d}\Gamma,\quad \mathbf{G}_e=\int_{\Gamma_e}\mathbf{Q}_e^{\mathrm{T}}\tilde{\mathbf{N}}_e\,\mathrm{d}\Gamma,\quad \mathbf{P}_e=\int_{eq}\tilde{\mathbf{N}}_e^{\mathrm{T}}\bar{q}_e\,\mathrm{d}\Gamma \tag{10}$$

The stationary condition is used to derive the element stiffness equation

$$\mathbf{K}_e\mathbf{d}_e=\mathbf{P}_e \tag{11}$$

where $\mathbf{K}_e=\mathbf{G}_e^{\mathrm{T}}\mathbf{H}_e^{-1}\mathbf{G}_e$ is stiffness matrix, $\mathbf{P}_e$ represents equivalent nodal thermal load vector. Then, assembling each element stiffness equation to obtain the total stiffness equation

$$\mathbf{Kd} = \mathbf{P} \tag{12}$$

2.3. Inverse Problems

When addressing the inverse boundary condition problem, most existing algorithms typically employ an iterative process for computation. However, the proposed algorithm in this paper introduces a novel scheme by directly determining the unknown boundary condition without resorting to iteration. The core concept of the proposed method can be concisely summarized as the following two steps:

Step 1. Calculate the temperature $\mathbf{T}_m$ at measurement points.

The temperature values at the measurement points can be obtained by employing HT-FEM to solve the direct problem.

Step 2. Determine the unknown boundary conditions by solving for the temperatures of the internal boundary nodes.

The total stiffness equation (12) can be derived from the direct heat conduction problem, where the node temperature vector **d** can be expressed as three components: the temperature $\mathbf{T}_o$ at the exterior boundary Γ_o, the temperature $\mathbf{T}_d$ in the domain, and the temperature $\mathbf{T}_i$ of the interior boundary Γ_i.

$$\begin{aligned}\mathbf{d} &= \left\{T_1, T_2, \cdots, T_o, T_{o+1}, \cdots, T_{o+d}, T_{o+d+1}, \cdots, T_{o+d+i}\right\}^{\mathbf{T}} \\ &= \left\{\left\{\mathbf{T}_o\right\}_{o\times 1}, \left\{\mathbf{T}_d\right\}_{d\times 1}, \left\{\mathbf{T}_i\right\}_{i\times 1}\right\}^{\mathbf{T}}\end{aligned} \tag{13}$$

Similarly, the stiffness matrix **K** can be partitioned as

$$\mathbf{K} = \left[\left(\mathbf{K}_1\right)_{d\times o}, \left(\mathbf{K}_2\right)_{d\times d}, \left(\mathbf{K}_3\right)_{d\times i}\right] \tag{14}$$

So,

$$\mathbf{Kd} = \mathbf{K}_1\mathbf{T}_o + \mathbf{K}_2\mathbf{T}_d + \mathbf{K}_3\mathbf{T}_i = \mathbf{P} \tag{15}$$

Furthermore, the node temperature in the intra-domain can be given by

$$(\mathbf{T}_d)_{d\times 1} = (\mathbf{K}_2^{-1})_{d\times d}\mathbf{P}_{d\times 1} - (\mathbf{K}_2^{-1}\mathbf{K}_1)_{d\times o}(\mathbf{T}_o)_{o\times 1} - (\mathbf{K}_2^{-1}\mathbf{K}_3)_{d\times i}(\mathbf{T}_i)_{i\times 1} \tag{16}$$

Then, the estimated temperature of measurement points can be manipulated as follows

$$\mathbf{T}_a = \mathbf{AP} - \mathbf{BT}_o - \mathbf{CT}_i \tag{17}$$

where **A, B** and **C** represent the sub matrices of $\mathbf{K}_2^{-1}$, $\mathbf{K}_2^{-1}\mathbf{K}_1$ and $\mathbf{K}_2^{-1}\mathbf{K}_3$ respectively. The objective function **F** is defined as the difference between the estimated temperature $\mathbf{T}_a$ and measurement temperature $\mathbf{T}_m$

$$\mathbf{F} = (\mathbf{T}_a - \mathbf{T}_m)^{\mathbf{T}}(\mathbf{T}_a - \mathbf{T}_m) \tag{18}$$

substituting Eq. (17) into (18) yields

$$\mathbf{F} = (\mathbf{AP} - \mathbf{BT}_o - \mathbf{CT}_i - \mathbf{T}_m)^{\mathbf{T}}(\mathbf{AP} - \mathbf{BT}_o - \mathbf{CT}_i - \mathbf{T}_m) \tag{19}$$

The unknown temperature $\mathbf{T}_i$ at the inner boundary node can be determined by taking the first-order partial derivative of objective function **F** with respect to $\mathbf{T}_i$ equal to zero

$$\frac{\partial \mathbf{F}}{\partial \mathbf{T}_i} = 0 \tag{20}$$

Further, $\mathbf{T}_i$ can be written as

$$\mathbf{T}_i = (\mathbf{C}^{\mathbf{T}}\mathbf{C})^{-1}\mathbf{C}^{\mathbf{T}}(\mathbf{AP} - \mathbf{BT}_o - \mathbf{T}_m) \tag{21}$$

For the identification of heat flux on the pipeline's inner boundary, we first determine

temperature of the inner wall based on the previous derivation. Then, we solve the direct problem once again by combining the known boundary conditions and the established inner temperature to identify the unknown inner heat flux.

The flowchart depicting the algorithm is presented in **Figure 3**.

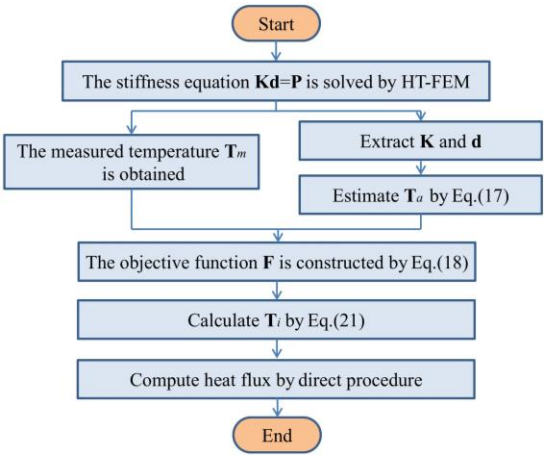

Figure 3. Flowchart of the inverse process

3. Numerical examples

To comprehensively evaluate the performance of the proposed algorithm in identifying boundary conditions, several numerical examples are considered. A comprehensive analysis is conducted to investigate the effects of the number of measurement point, their location, and measurement error on the inversion results. The average relative error can be given by

$$ARE = \sqrt{\sum_{i=1}^{N}\left(T_{inv}-T_{exa}\right)_i^2 \Big/ \sum_{i=1}^{N}\left(T_{exa}\right)_i^2}\times 100\% \tag{22}$$

the relative error is indicated as

$$RE = \left|\frac{T_{inv}-T_{exa}}{T_{exa}}\right|\times 100\% \tag{23}$$

where T_{inv} and T_{exa} represent the inverse and exact temperature of the unknown boundary, respectively, N denotes the number of nodes.

3.1. Identification of boundary conditions for circular pipeline

As illustrated in **Figure 4**, we analyzed a circular-ring pipeline model. In this model, the inner boundary geometry is a circle of radius 0.25, and the outer boundary shape is a circle with a radius of 1. The outer boundary condition is specified, whereas the inner boundary condition remains unknown. The whole solution domain adheres to an analytical solution $T = 2x_1^2 - x_2^2$. The finite element model is divided into 96 linear elements containing 112 nodes. The thermal conductivity values are $k_{11}=1$ and $k_{22}=2$. In this analysis, we investigate the effect of the number of measurement points on inverse results. **Figure 4** presents three distinct sets of measurement points, with *m*= 4, 8, and 16, respectively.

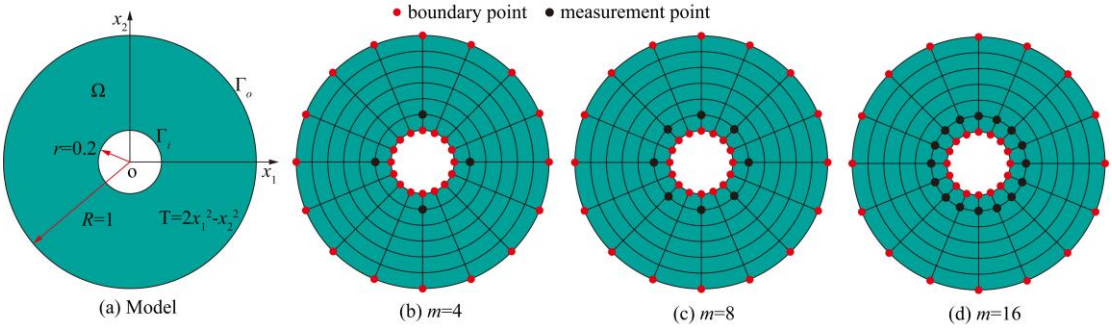

Figure 4. Geometry model and different number of measurement points

Figure 5 displays the inversion results obtained with varying numbers of measurement points, while their corresponding relative errors are shown in **Figure 6**. It can be seen from these graphs that as the number of measurement points increases, the inversion results converge more closely to the exact solution. **Table 1** presents the ARE between the inverse and exact solutions for different numbers of measurement points. Notably, the inverse results demonstrate higher accuracy when the number of measurement points is configured as 16, with an inversion deviation of merely 1.351e-3. The computational process is implemented on a computer equipped with an Intel (R) Core (TM) i7-11700F @2.50GHz CPU and 16 GB of system memory. The computational time of the proposed method is only about 0.0068 second for the example, showing high efficiency in practical applications.

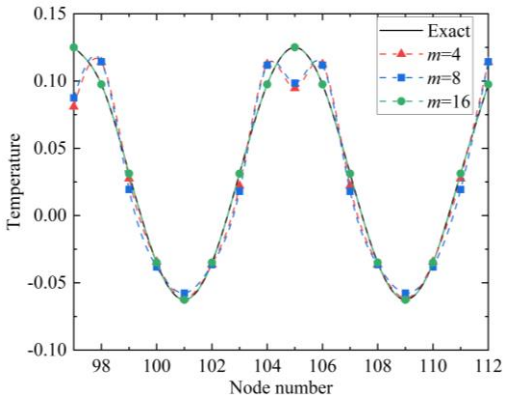

Figure 5. Inverse results for different number of measurement points

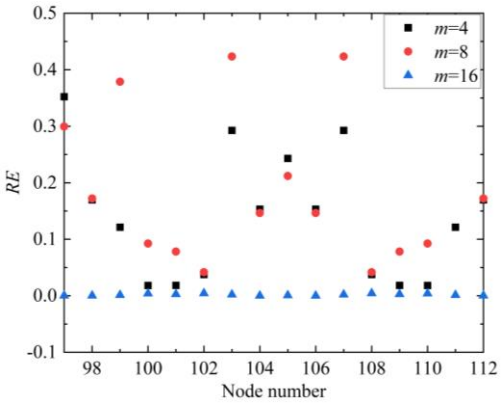

Figure 6. Relative error of inverse results for different number of measurement points

Table 1 *ARE* under the different number of measurement points

Number of measurement points	4	8	16
ARE	2.174e-1	2.097e-1	1.351e-3

3.2. Identification of boundary conditions for elliptic pipeline

As depicted in **Figure 7 (a)**, a pipeline model characterized by an elliptic ring-shaped cross-section is taken into consideration. The outer boundary geometry of the model is elliptical, with a long semi-axis of 6 and a short semi-axis of 4. A precisely defined temperature boundary condition $T_o = 10$ is imposed on the outer boundary of the studied

domain. The inner boundary shape is formed by an ellipse with a long semi-axis of 3 and a short semi-axis of 2. The temperature at inner boundary is unknown. Nevertheless, it is assumed to adhere to the specific temperature $T_i = \sin(x_1 + x_2)$. The thermal conductivity values are determined to be $k_{11} = 1$ and $k_{22} = 3$. The entire computational domain is discretized into 80 linear elements, which are associated with 96 nodes in total. 16 measurement points are utilized to perform the computational analysis. Here, the effect of the locations of the measurement points on inverse results is discussed. **Figure 7 (b-e)** displays four sets of measurement points at different positions.

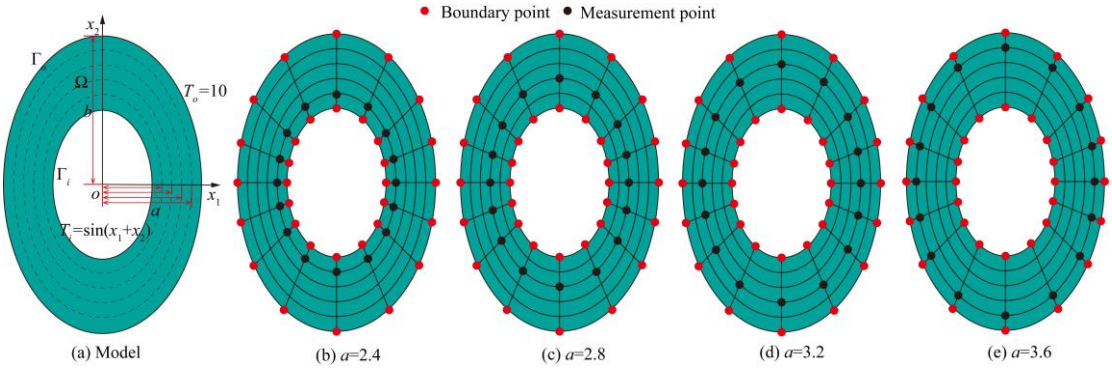

Figure 7. Geometry model and different locations of measurement points

Figure 8 illustrates the inversion results obtained for various positions of measurement points, while their relative errors are depicted in **Figure 9**. The ARE between the inverse solution and actual solution for the different locations of measurement points are presented in **Table 2**. From these results, it can be clearly seen that the closer measurement points are to the target boundary, the more accurate the inversion results are. It is worth noting that each configuration of measurement point locations can achieve relatively accurate inversion results, which reflects the stability of the proposed method. Meanwhile, the calculation takes 0.0011 second.

Table 2 *ARE* under the different location of measurement points

Location of measurement points	a=2.4	a=2.8	a=3.2	a=3.6
ARE	5.630e-4	4.472e-3	6.138e-3	7.751e-2

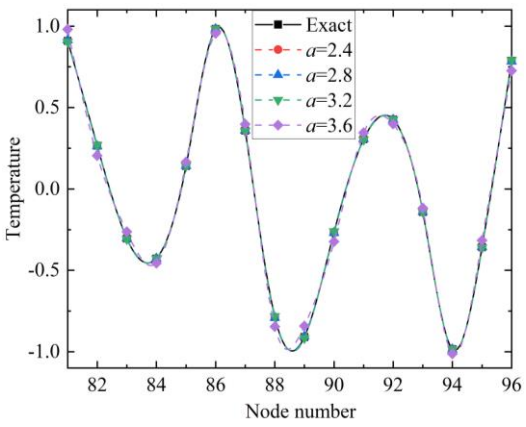

Figure 8. Inverse results for different locations of measurement points

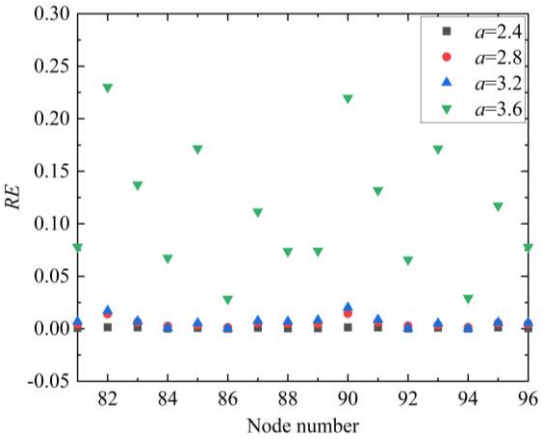

Figure 9. Relative error of inverse results for different locations of measurement points

3.3. Pipeline with square ring section

The measured temperature at measurement points is obtained through a direct procedure, which often introduces measurement errors during calculation. Therefore, to better align with practical scenarios, the effect of measurement error on inverse results is considered.

$$\mathbf{T}_m^{'} = \mathbf{T}_m + \varepsilon\boldsymbol{\omega} \tag{24}$$

where $\mathbf{T}_m$ denotes the temperature at measurement points from direct problem, ε is the standard deviation of measurement errors, and $\boldsymbol{\omega}$ denotes a vector with random variables that follow a uniform distribution.

As illustrated in **Figure 10**, we consider a pipeline with a square ring section. The outer boundary geometry takes the shape of a square with a side length of 6, while the inner boundary forms a square with a side length of 2. The outer boundary condition is explicitly defined, whereas the inner boundary condition remains unknown and represents the quantities to be identified. The entire computational domain has an analytical solution for the temperature $T = -10x_1^2 + 2x_2^2 + 3x_1x_2 + 4x_1 + 5x_2 + 6$. The thermal conductivities are $k_{11} = 1$ and $k_{22} = 5$. The entire model is partitioned into 160 linear elements with 180 nodes. 20 measurement points are selected for analysis, as shown in **Figure 10 (b)**.

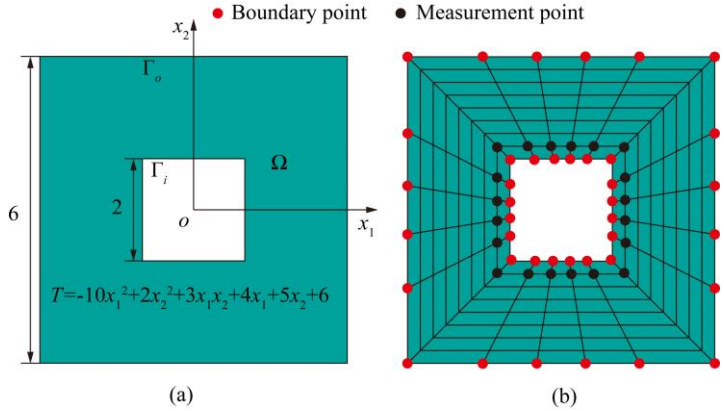

Figure 10. Geometry model and meshing

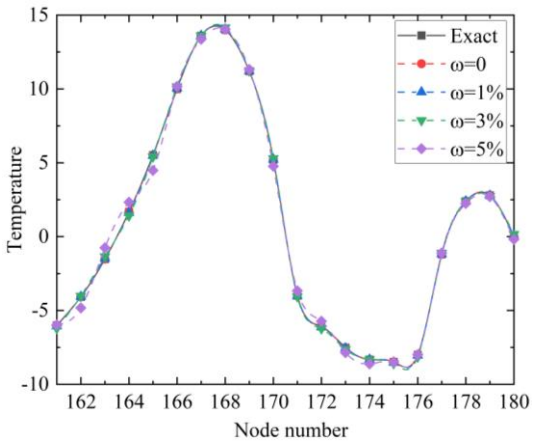

Figure 11. Inverse results for different measurement errors

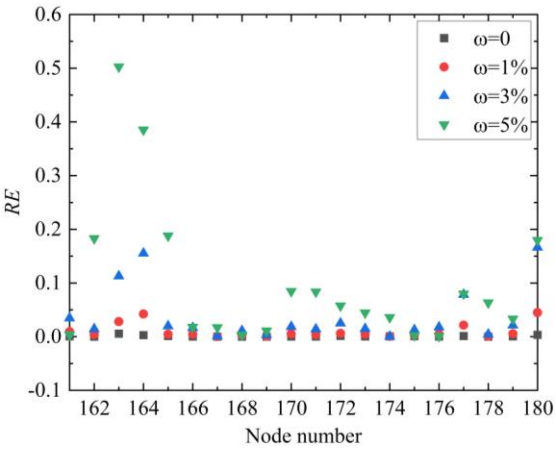

Figure 12. Relative error of inverse results for different measurement errors

Figures 11 and **12** depict the inversion results and their corresponding relative errors for measurement errors of 1%, 3%, and 5%, respectively. **Figure 13** displays the overall average relative error for different measurement errors. It can be found that as the measurement errors increase, the inversion results gradually deviate from the exact solution. Notably, even when the measurement error reaches 5%, the overall average relative error is merely 5.719e-2, which reflects that the proposed method exhibits low sensitivity to measurement errors. In this example, the computational time is only 0.0064 second.

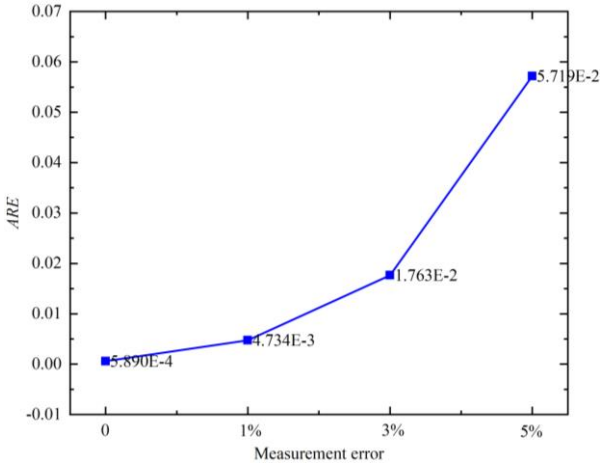

Figure 13. *ARE* of inverse results for the different measurement errors

3.4. Pipeline with quadrangle gyro ring section

A pipeline model with a quadrangle gyro ring section is considered as depicted in **Figure 14**. The outer boundary is formed by the intersection of two ellipses, each with a long-axis of b_1=2 and a short-axis of a_1=1.5. Similarly, the inner boundary is defied by the intersection of two ellipses, each with a long-axis of b_2=1 and a short-axis of a_2=0.75. 80 linear elements with 96 nodes are adopted to discretize the solution model. The thermal conductivities considered are represented by $k_{11}=1$ and $k_{22}=3$. The outer boundary condition imposes a constant temperature $T_o=10$. The inner boundary condition is unknown and is presumed to conform to the actual heat flux boundary condition, denoted as $q_i=50\sin(x_1+x_2)$.

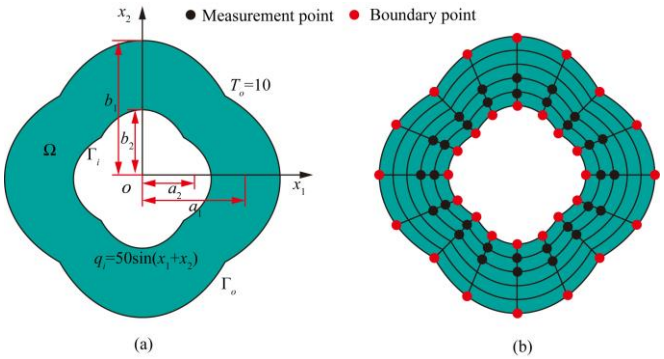

Figure 14. Geometry model and meshing

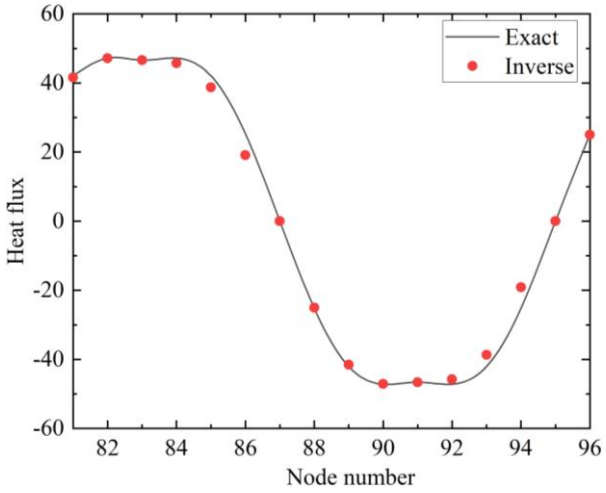

Figure 15. Inverse results and exact solution

Figure 15 shows the comparison between the inverse heat flux results and actual solutions. It can be observed that the inverse results are in excellent agreement with the actual solutions. Meanwhile, the computational time is 0.0052 second. This indicates that the proposed method retains high computational accuracy and effectiveness in handling mixed boundary conditions and directly identifying heat flux boundary conditions.

4. Conclusions

An efficient non-iterative algorithm grounded in HT-FEM is developed for identifying thermal boundary conditions of the inner walls of pipeline in orthotropic media. The key of this algorithm is the extraction and manipulation of the finite element stiffness matrix, eliminating the need for any iterative processes during computation. Consequently, it achieves high computational efficiency when solving inverse problems. The objective function is formulated by the deviation between the measured temperature and evaluated temperature at measurement points. The evaluated temperature can be derived as a function of the unknown temperatures at the boundary nodes. Minimizing the objective function enables directly identification of the unknown boundary conditions. Several numerical examples are meticulously analyzed to investigate the effects of various factors, encompassing the number of measurement points, their positions, measurement errors, and mixed boundary conditions, on inversion results. The findings reveal that increasing the number of measurement points leads to more precise inversion results. The greater the proximity of measurement points to the boundary that requires identification, the higher precision of the inversion result. With the increase in measurement error, the identification deviation gradually rises, but the identification result remains reliable. Additionally, satisfactory inversion results can also be obtained under mixed boundary conditions. This demonstrates that the proposed method exhibits remarkable inversion accuracy and identification efficiency in identifying thermal boundary conditions for the orthotropic heat conduction problem.

Acknowledgements

This work is supported by the National Natural Science Foundation of China (grant number: 12572224) and the Natural Science Foundation of Anhui Province (grant number: 2408085MA015).

Nomenclature

A - submatrix of matrix $\mathbf{K}_2^{-1}$
B - submatrix of matrix $\mathbf{K}_2^{-1}\mathbf{K}_1$
C - submatrix of matrix $\mathbf{K}_2^{-1}\mathbf{K}_3$
$\mathbf{c}_e$ - undetermined coefficients
d - node temperature vector
F - objective function
k_{11}, k_{22} - thermal conductivity
K - thermal stiffness matrix
$\mathbf{K}_1, \mathbf{K}_2, \mathbf{K}_3$ - submatrix of **K**
$\mathbf{N}_e$ - complete solution
$\tilde{\mathbf{N}}_e$ - frame shape function vector
n - number of terms of complete solution
N - number of nodes
P - equivalent thermal load vector
q - heat flux
$\bar{q}$ - heat flux boundary condition
T - temperature
$\bar{T}_o$ - outer boundary temperature
$\bar{T}_i$ - inner boundary temperature
$\mathbf{T}_a$ - estimated temperature
$\mathbf{T}_m$ - measurement temperature
$\tilde{T}_e$ - frame temperature
x_1, x_2 - coordinates

Abbreviation

ARE - average relative error
RE - relative error

Greek symbols

Γ_o - outer boundary
Γ_i - inner boundary
Ω - solution domain
Π_m - variational functional
ε - measurement error
ω - random variable

References

[1] Monde, M., Analytical method in inverse heat transfer problem using Laplace transform technique, *International Journal of Heat and Mass Transfer, 43* (2000), pp. 3965-3975.

[2] Zwicke, F., Elgeti, S., Inverse design based on nonlinear thermoelastic material models applied to injection molding, *Finite Elements in Analysis and Design, 165* (2019), pp. 65-76.

[3] Ling, X. W., *et al.*, A non-iterative finite element method for inverse heat conduction problems, *International Journal for Numerical Methods in Engineering, 56* (2023), pp. 1315-1334.

[4] Murio, D. A., The mollification method and the numerical solution of the inverse heat conduction problem by finite differences, *Computers Mathematics with Applications, 17* (1989), pp. 1385-1396.

[5] Yu, G. X., *et al.*, Meshless inverse method to determine temperature and heat flux at boundaries for 2D steady-state heat conduction problems, *Experimental Thermal and Fluid Science, 52* (2014), pp. 156-163.

[6] Singh, K. M., Tanaka, M., Dual reciprocity boundary element analysis of inverse heat conduction problems, *Computer Methods in Applied Mechanics and Engineering, 190* (2001), pp. 5283-5295.

[7] Liu, X., *et al.*, A virtual boundary element method for three-dimensional inverse heat conduction problems in orthotropic media, *CMES-Computer Modelling in Engineering Sciences, 117* (2018), pp. 189-211.

[8] Qiu, W. K., *et al.,* A novel hybrid deep learning algorithm for estimating temperature-dependent thermal conductivity in transient heat conduction problems, *International Communications in Heat and Mass Transfer, 164* (2025), pp. 108871.

[9] Liu, C. S., An efficient simultaneous estimation of temperature-dependent thermophysical properties, *CMES-Computer Modelling in Engineering Sciences, 14* (2006), pp. 77-90.

[10] Somasundharam, S., Reddy, K. S., Inverse analysis for simultaneous estimation of temperature dependent thermal properties of isotropic materials, *Thermal Science and Engineering Progress, 20* (2020), pp. 100728.

[11] Gu, Y., *et al.,* Application of the meshless generalized finite difference method to inverse heat source problems, *International Journal of Heat and Mass Transfer, 108* (2017), pp. 721-729.

[12] Kazemzadeh-Parsi, M. J., Daneshmand, F., Solution of geometric inverse heat conduction problems by smoothed fixed grid finite element method, *Finite Elements in Analysis and Design, 45* (2009), pp. 599-611.

[13] Jiang, G. H., *et al.,* Shape reconstruction in transient heat conduction problems based on radial integration boundary element method, *International Journal of Heat and Mass Transfer, 191* (2022), pp. 122830.

[14] Vaka, A. S., *et al.,* Novel inverse heat transfer methodology for estimation of unknown interfacial heat flux of a continuous casting mould: A complete three- dimensional thermal analysis of an industrial slab mould, *International Journal of Thermal Sciences, 160* (2021), pp. 106648.

[15] Qiu, W. K., *et al.,* Estimating the boundary conditions for 3D transient heat conduction by bidirectional long short-term memory network and attention mechanism, *International Journal of Heat and Mass Transfer, 233* (2024), pp. 126042.

[16] Wang, H., Qin, Q. H., Hybrid FEM with fundamental solutions as trial functions for heat conduction simulation, *Acta Mechanica Solida Sinica, 22* (2009), pp. 487-498.

[17] Qiu, W. K., *et al.,* Hybrid finite element analysis of heat conduction in orthotropic media with variable thermal conductivities, *International Journal of Applied Mechanics 12* (2020), pp. 2050098.

[18] Qiu, W. K., *et al.,* A special corner element for solving heat conduction problems, *International Journal of Computational Methods, 22* (2025), pp. 2450058.

[19] She, Z., *et al.,* Thermal analysis of multilayer coated fiber-reinforced composites by the hybrid Trefftz finite element method, *Composite Structures, 224* (2019), pp. 110992.

[20] Karnal, M., Batul, B., Estimation of exhaust gas temperature of the rocket nozzle using hybrid approach, *Journal of Thermal Science, 25* (2016), pp. 485-491.

[21] Frąckowiak, A., *et al.,* Trefftz numerical functions for solving inverse heat conduction problems, *International Journal of Thermal Sciences, 177* (2022), pp. 107566.

[22] Sun, Y., He, S. N., A meshless method based on the method of fundamental solution for three-dimensional inverse heat conduction problems, *International Journal of Heat and Mass Transfer, 108* (2017), pp. 945-960.

[23] Tourn, B. A., *et al.,* Implementation of total variation regularization-based approaches in the solution of linear inverse heat conduction problems concerning the estimation of surface heat fluxes, *International Communications in Heat and Mass Transfer, 125* (2021), pp. 105330.

[24] Chen, H. L., *et al.,* Identification of transient boundary conditions with improved cuckoo search algorithm and polynomial approximation, *Engineering Analysis with Boundary Elements, 95* (2018), pp. 124-141.

[25] Wang, X. Y., *et al.,* Inverse identification of temperature-dependent thermal conductivity for charring ablators, *International Journal of Thermophysics, 42* (2021), pp. 26.

[26] Udayraj, *et al.,* Performance analysis and feasibility study of ant colony optimization, particle swarm optimization and cuckoo search algorithms for inverse heat transfer problems, *International Journal of Heat and Mass Transfer, 89* (2015), pp. 359-378.

[27] Sun, S. C., *et al.,* Inverse identification of temperature-dependent thermal properties using improved Krill Herd algorithm, *International Journal of Thermophysics, 39* (2018), pp. 121.

[28] Yang, K., *et al.,* A new modified conjugate gradient method to identify thermal conductivity of transient non-homogeneous problems based on radial integration boundary element method, *International Journal of Heat and Mass Transfer, 133* (2019), pp. 669-676.

[29] Ghadimi, B., *et al.,* Heat flux on-line estimation in a locomotive brake disc using artificial neural networks, *International Journal of Thermal Sciences, 90* (2015), pp.203-213.

[30] Gu, J. H., *et al.,* A fast inversion approach for the identification of highly transient surface heat flux based on the generative adversarial network, *Applied Thermal Engineering, 220* (2023), pp. 119765.

[31] Su, C. R., Chen, C. K., Geometry estimation of the furnace inner wall by an inverse approach, *International Journal of Heat and Mass Transfer, 50* (2007), pp. 3767-3773.

[32] Su, C. R., *et al.,* Estimation for inner surface geometry of furnace wall using inverse process combined with grey prediction model, *International Journal of Heat and Mass Transfer, 52* (2009), pp. 3595-3605.

[33] Yu, B., *et al.,* A novel non-iterative inverse method for estimating boundary condition of the furnace inner wall, *International Communications in Heat and Mass Transfer, 87* (2017), pp. 91-97.

[34] Qiu WK, *et al.,* Boundary geometry reconstruction for orthotropic heat conduction problems based on HT-FEM, *Numerical Heat Transfer Part B-Fundamentals, 86* (2025), pp. 87-105.

- Paper submitted: 07 December 2025
- Paper revised: 04 March 2026
- Paper accepted: 06 March 2026